17th Brazilian Congress of Thermal Sciences and Engineering
November 25th-28th, 2018, Águas de Lindóia, SP, Brazil

ENCIT-2018-0523

CONVECTION STUDY IN A SQUARE CAVITY USING LATTICE BOLTZMANN METHOD

Luiz Eduardo Czelusniak
Vinícius Pessoa Mapelli
Luben Cabezas-Gómez
Escola de Engenharia de São Carlos, Universidade de São Paulo, Avenida Trabalhador são-carlense, 400 - Parque Arnold Schimidt, São Carlos - SP, 13566-590, Brazil
luiz.czelusniak@usp.br, vinicius.mapelli@usp.br, lubencg@sc.usp.br

Matheus dos Santos Guzella
Instituto de Ciência e Tecnologia, Universidade Federal dos Vales do Jequitinhonha e Mucurí, Rodovia MGT 367, km 583, nº 5000 Alto da Jacuba, Diamantina - MG, 39100-000 , Brazil
matheus.guzella@ict.ufvjm.edu.br

Abstract. *Fluid flows and heat transfer processes inside cavities has been an active study field due to its geometry simplicity and capability of reaching complex regimes, presenting vortices and recirculation. Since this problem has usual occurrence in engineering applications, many researchers have assessed square cavities using different numerical simulation approaches. In this context, Lattice-Boltzmann method (LBM) is one of the tools that has gained space in academy over the past two decades. In the present work, Lattice Boltzmann methods are used to solve mass, momentum and energy conservation equations by solving the evolution in time of two distribution functions. A square cavity with a length of size H = L and one inlet and outlet port, sized to W = 0.25H, is assessed in different hydrodynamic and thermal conditions. Two distinct LBM methodologies were assessed for this problem: first one solves energy conservation equation as an advection-diffusion of temperature and second one has its formulation based upon total energy field. Numerical results of streamlines, temperature fields, average and local Nusselt number, and dimensionless drop are presented for different flow conditions. Both methodologies were able to capture interesting characteristics of the flow, such as vortices and general trend of local Nusselt number. Further studies are needed to draw deeper conclusions.*

Keywords: *Forced convection, Lattice Boltzmann Method, Numerical Simulation.*

1. INTRODUCTION

Fluid flows and heat transfer processes inside cavities has been an active study field because of the characteristics this sort of problem presents. The main one is its occurrence in several engineering applications, such as heat exchangers, lubrification technology, drying technology, electronics cooling, ventilation of rooms and solar storage (Mioralli *et al.*, 2017). The second reason is its geometry simplicity, which allows researchers use different approaches to this type of problem such as analytical (Bejan, 1980) and numerical solutions (Peng *et al.*, 2003; Guo *et al.*, 2007). Although its geometry simplicity, flows inside cavities can reach complex regimes, presenting vortices and recirculation. And that turns flows inside cavities a very interesting benchmark to check numerical stability and conservation of variables such as mass, momentum and energy.

In numerical methods context, Lattice-Boltzmann method (LBM) is one of the approaches that has gained space in academy over the past two decades. It has shown great potential to solve a range variety of hydrodynamic flows, such as porous media (Guo and Zhao, 2002) , acoustics (Brès *et al.*, 2009), multiphase (He *et al.*, 1999) , incompressible and even flows with shock waves (Guangwu *et al.*, 1999) and turbulence (Yu *et al.*, 2005; Chen *et al.*, 2004). Although it has shown great performance in isothermal flows, its application to thermal flows is not straightforward. When applied to solving heat transfer flow problems, thermal LBM (TLBM) methods has shown severe instability, limiting TLBM to flows of relatively small Reynolds number. However, many researchers have been working on different strategies to overcome this drawback. The existing TLBM models can be classified into three categories. The first one is to approach temperature as passive scalar, which is advected by velocity field but does not affect flow fields (density or velocity fields) (Lallemand and Luo, 2003). The second category of TLBM consider solving fully compressible Euler or Navier-Stokes equations, by using interpolation advection, by including finite-difference scheme for solving discrete velocity models or by using a larger set of discrete velocities in order to recover continuous energy conservation

equation. The third category of TLBM solves the evolution of traditional velocity distribution function (governed by Boltzmann equation) along with the evolution of a distribution function related to thermal field. For example, He *et al.* (1998) developed a TLBM capable of solving thermal flows including viscous dissipation and pressure work effects. Later, Guo *et al.* (2007) showed a TLBM based on total energy instead of internal energy, what increased locality and numerical stability of results. Also, Chen *et al.* (2012) developed a TLBM based on total enthalpy, which is a common variable in combustion research field.

In the present work, it is proposed to apply TLBM methods to square cavity problems involving forced convection for different hydrodynamic and thermal conditions, using distinct methodologies. Results are compared with traditional CFD results available in literature.

2. METHODS

2.1 Problem description

The proposed problem is based on the work of Mioralli *et al*. (2017). It consists of an incompressible flow inside a two-dimensional square cavity. The cavity has a length of size H = L, one inlet port and one outlet port, both of size W = 0.25 H. The walls of the cavity are subject to a constant temperature of T_w. The fluid flows into the cavity with assuming uniform velocity and temperature profiles of u_{in} and T_{in} . A schematic drawing of the cavity is shown in Fig. 1.

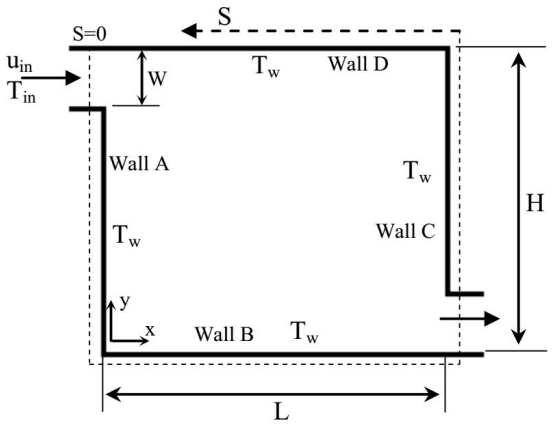

Figure 1. Schematic drawing of the square cavity (Mioralli *et al*., 2017).

2.2 Governing Equations

To reproduce the mass, momentum and energy conservation equations with the LBM, it was used two distribution functions: one distribution function f to reproduce the mass and momentum conservation equations and a second distribution function g to reproduce the energy conservation equation, discretized in 9 velocities (D2Q9), following two different approaches.

2.2.1 Methodology 1

In both approaches, evolution of distribution function f in time is governed by discretized Boltzmann equation, also known as Lattice-Boltzmann equation:

$$f_i(\mathbf{x} + \mathbf{c_i}\Delta t, t + \Delta t) = f_i(\mathbf{x}, t) + \frac{\Delta t}{\tau_f}[f_i^{eq}(\mathbf{x}, t) - f_i(\mathbf{x}, t)] \tag{1}$$

Where τf is the relaxation parameter. In this approach, incompressible equilibrium distribution function f^{eq} is computed as described in Eq. (2):

$$f_i^{eq} = w_i\rho + w_i\rho_0\left(\frac{\mathbf{c_i}\cdot\mathbf{u}}{c_s^2} + \frac{(\mathbf{c_i}\cdot\mathbf{u})^2}{2c_s^4} - \frac{\mathbf{u}\cdot\mathbf{u}}{2c_s^2}\right) \tag{2}$$

Where ρ is the variable related to pressure variation, ρ_0 is the fluid density and **u** is the velocity field. Discretized velocity vector $\mathbf{c}_i$ is defined according to the following D2Q9 lattice:

$$\mathbf{c_i} = \begin{cases} [0,0] & i = 0 \\ c\left[\cos\left((i-1)\frac{\pi}{2}\right), \sin\left((i-1)\frac{\pi}{2}\right)\right] & i = 1,2,3,4 \\ c\left[\cos\left((i-\frac{9}{2})\frac{\pi}{2}\right), \sin\left((i-\frac{9}{2})\frac{\pi}{2}\right)\right] & i = 5,6,7,8 \end{cases} \tag{3}$$

Where c = Δx/Δt and $c_s^2 = c$ is the lattice sound speed. The weight coefficients corresponding to discretized velocities are $w_0 = 4/9$, $w_{1\,\mathrm{to}\,4} = 1/9$, and $w_{5\,\mathrm{to}\,9} = 1/36$. For the advection-diffusion Lattice Boltzmann equation, equilibrium distribution g^{eq} is given by:

$$g_i^{eq} = w_i T\left(1 + \frac{\mathbf{c_i}\cdot\mathbf{u}}{c_s^2}\right) \tag{4}$$

And its evolution in time is solved the same way distribution function f, as described in Eq. (1).

The correspondence between the LB equations and the related conservation equations can be done through a Chapman-Enskog analysis (Krüger *et al*., 2017), from where it is possible to determine relation between the relaxation parameter and transport coefficients, given by:

$$\nu = \frac{1}{3}\left(\frac{\tau_f}{\Delta t} - \frac{1}{2}\right)\frac{\Delta x^2}{\Delta t}, \quad \alpha = \frac{1}{3}\left(\frac{\tau_g}{\Delta t} - \frac{1}{2}\right)\frac{\Delta x^2}{\Delta t} \tag{5}$$

Where ν is the kinematic viscosity, and α is thermal diffusivity. Velocity and temperature fields can be retrieved computing moments of distribution functions, as described in Eq. (6).

$$\rho_0 = \sum_i f_i, \quad \rho\mathbf{u} = \sum_i f_i\mathbf{c_i}, \quad T = \sum_i g_i \tag{6}$$

Also, Chapman-Enskog analysis allows to recover macroscopic governing equations when solving both distribution functions. The resultant steady state governing equations from this methodology for density, momentum and temperature are shown from Eq. (7) to Eq. (9).

$$\nabla\cdot\mathbf{u} = 0 \tag{7}$$

$$\rho_o\nabla\cdot(\mathbf{uu}) = -\nabla p + \mu\nabla\cdot(\mathbf{S}) \tag{8}$$

$$\nabla\cdot(\mathbf{u}T) = \nabla(\alpha\nabla T) \tag{9}$$

where $\mathbf{S} = [\nabla\mathbf{u} + (\nabla\mathbf{u})^T]$. The Reynolds number for this flow is defined as $Re = \rho_0 u_{in} H/\mu$.

2.2.2 Methodology 2

As a second approach, a model developed by Guo *et al.* (2007) was used to solve forced convection by relating distribution function g to total energy density field, E.

In this methodology, temporal evolution of distribution function f is solved as in Eq. (1), using compressible equilibrium distribution f^{eq} :

$$f_i^{eq} = w_i\rho\left(1 + \frac{\mathbf{c_i}\cdot\mathbf{u}}{c_s^2} + \frac{(\mathbf{c_i}\cdot\mathbf{u})^2}{2c_s^4} - \frac{\mathbf{u}\cdot\mathbf{u}}{2c_s^2}\right) \tag{10}$$

Although this equilibrium distribution function recovers compressible macroscopic equations, compressibility effects can be minimized depending on simulation parameters. In summary, it is desirable that velocities are much lower than lattice speed sound c_s^2 (Guo *et al.,* 2007; Krüger *et al.,* 2017).

Temporal evolution of distribution g is described in Eq. (11).

$$g_i(\mathbf{x}+\mathbf{c_i}\Delta t, t+\Delta t) = g_i(\mathbf{x},t) + \frac{\Delta t}{\tau_f}[g_i^{eq}(\mathbf{x},t) - g_i(\mathbf{x},t)] + \Delta t\left(1-\frac{\Delta t}{2\tau_g}\right)\frac{Z_i}{\tau_{gf}}(f_i - f_i^{eq}) \tag{11}$$

where

$$\frac{1}{\tau_{gf}} = \frac{1}{\tau_g} - \frac{1}{\tau_f} \tag{12}$$

and

$$Z_i = \mathbf{c_i}\cdot\mathbf{u} - \frac{\mathbf{u}\cdot\mathbf{u}}{2} \tag{13}$$

Equilibrium distribution function g^{eq} is computed as described in Eq. (14) (Guo *et al.*, 2007):

$$g_i^{eq} = w_i\rho c_s^2\left[\frac{\mathbf{c}_i\cdot\mathbf{u}}{c_s^2} + \left(\frac{\mathbf{c}_i\cdot\mathbf{u}}{c_s^2}\right)^2 - \frac{\mathbf{u}\cdot\mathbf{u}}{c_s^2} + \frac{1}{2}\left(\frac{\mathbf{c}_i\cdot\mathbf{c}_i}{c_s^2} - D\right)\right] + Ef_i^{eq} \tag{14}$$

where D is number of dimensions considered in solution, which is considered bidimensional in the present work. Through Chapman-Enskog analysis, it is possible to show this methodology leads to macroscopic equations as described from Eq. (15) to Eq. (17) (Guo *et al.*, 2007).

$$\partial_t\rho + \nabla\cdot(\rho\mathbf{u}) = 0 \tag{15}$$

$$\partial_t(\rho\mathbf{u}) + \nabla\cdot(\rho\mathbf{u}\mathbf{u}) = -\nabla p + \nabla\cdot(\mu\mathbf{S}) \tag{16}$$

$$\partial_t(\rho E) + \nabla\cdot[(p+\rho E)\mathbf{u}] = \nabla\cdot(\alpha\nabla T) + \nabla\cdot(\mu\mathbf{S}\cdot\mathbf{u}) \tag{17}$$

Transport coefficients μ and α follows same relations as in Eq. (5). To maintain consistency between both methodologies, an Eckert number $Ec = 10^{-30}$ (Guo *et al.,* 2007) was assumed in order to maintain viscous effects in energy equation negligible. Compression work effects can be neglected when velocities simulated are considerable lower than lattice speed sound. In this methodology, it was possible to keep $|\mathbf{u}|/c_s^2$ lower than 0.04, except when Re = 500, in which incompressible equilibrium function was used. Also transport coefficients were assumed constant, and numerical simulations were performed until steady state were reached.

2.3 Boundary conditions

2.3.1 Methodology 1

To assure inlet velocities and no-slip condition at walls, bounce-back rules (Ladd and Verberg, 2001) were applied as it is described in Eq. (18).

$$f_{\bar{i}}(\mathbf{x}_b, t+\Delta t) = f_i^*(\mathbf{x}_b, t) - 2w_i\rho_w\frac{\mathbf{c}_i\cdot\mathbf{u}_w}{c_s^2} \tag{18}$$

where subscript b indicates properties evaluated at boundary nodes, and subscript w properties evaluated at the wall location. Also. subscript $\bar{i}$ are related to discretized velocity $\mathbf{c}_{\bar{i}} = -\mathbf{c}_i$, and superscript * represents post collision populations.

A known pressure at outlet port is assured by using anti-bounce-back formulation (Ginzburg *et al.*, 2008) to the unknown populations at the boundary:

$$f_{\bar{i}}(\mathbf{x}_b, t+\Delta t) = -f_i^*(\mathbf{x}_b, t) + 2w_i\rho_w\left[1 + \frac{(\mathbf{c}_i\cdot\mathbf{u}_w)^2}{c_s^4} - \frac{\mathbf{u}_w^2}{2c_s^2}\right] \tag{19}$$

For distribution function g, an anti-bounce back developed by Ginzburg (2005) is applied to unknown populations at the boundary in order to assure Dirichlet conditions at inlet and at the cavity walls:

$$g_{\bar{i}}(\mathbf{x}_b, t+\Delta t) = -g_i^*(\mathbf{x}_b, t) + 2g_i^{eq}(\mathbf{x}_w, t+\Delta t) \tag{20}$$

At the outlet, a zero-gradient temperature in x direction is set by replacing all populations at the boundary nodes by its equilibrium value added to the non-equilibrium contribution extrapolated from adjacent node (Tang, 2005).

$$g_i = g_i^{eq}(\mathbf{x}_b, \mathbf{u}_w, T_w) + [g_i(\mathbf{x}_f) - g_i^{eq}(\mathbf{x}_f)] \tag{21}$$

In this case, macroscopic temperature at the outlet port used to compute equilibrium contribution is calculated by using a second order extrapolation.

2.3.2 Methodology 2

In the second approach, both distributions functions f e g at the boundaries were replaced following the non-equilibrium extrapolation (NEE) formulation described in Eq. (21). At the inlet and walls, where Dirichlet boundary conditions are imposed, application of NEE boundary condition is straightforward. At the outlet port, velocity $\mathbf{u}_w$ can be calculated by imposing known pressure and computing first and second moments using know populations values. Temperature T_w is calculated using a second order extrapolation from adjacent nodes.

2.4 Local and Average Nusselt Number

In order to represent the location of each point of the wall, it was defined an S coordinate system (Fig. 1) based on previous works in the literature (Saedi and Khodadadi, 2006; Mioralli *et al.*, 2017). The interval S = 0-1, represents the left side of the cavity, as well as the intervals (1-2), (3-4) and (4-1) represents, respectively, the bottom, right and top sides of the cavity.

A local Nusselt number is defined for each point of the walls, involving the intervals (0.25-1), (1-2), (2.25-3) and (3-4). Then the average Nusselt number for each wall is defined as follows:

$$\overline{Nu_i} = -\frac{1}{(S_{i1}-S_{i2})}\int_{S_{i1}}^{S_{i2}} Nu_i dS \tag{22}$$

where S_{i1} and S_{i2} are S-coordinates of the two ends of the ith wall.

The average Nusselt number for the whole cavity is computed as the weighted average of Nusselt numbers of each wall in relation with the walls sides.

$$\overline{Nu} = \sum_i \frac{\overline{Nu_i}(S_{i2}-S_{i1})}{S_{tot}} \tag{23}$$

2.5 Iterative error and tolerance

As a stopping criteria, the following quantity was calculated for every case:

$$\epsilon_\Phi = \sqrt{\frac{\sum_x(\Phi_k(\mathbf{x},t)-\Phi_{k-n}(\mathbf{x},t))}{\sum_x \Phi_{k-n}^2(\mathbf{x},t)}} \tag{24}$$

where Φ subscript indicates which field ϵ variable is related to (velocity or temperature), k indicates actual time step number, and n indicate number of previous time steps. In the present work, it was adopted $n = 100$, and $\epsilon < 10^{-6}$ for both velocity and temperature (energy) fields.

3. RESULTS

The velocity and temperature fields were obtained for a range of Prandtl and Reynolds numbers. After a convergence analysis, the local and average Nusselt numbers were studied for the cavity walls. Also, results for the coefficient of pressure drop, streamlines and temperature fields of the flow are shown in the present work.

3.1 Numerical Convergence

The first step of the work consisted in the analysis of the mesh size effects in the results obtained from simulations. For the methodology 1 with the prescribed boundary conditions, simulations were performed with an initial mesh size of 160 nodes in each size of the cavity and a grid refinement was conducted until convergence of the average Nusselt number was obtained. An example of the procedure adopted can be seen in Fig 2.

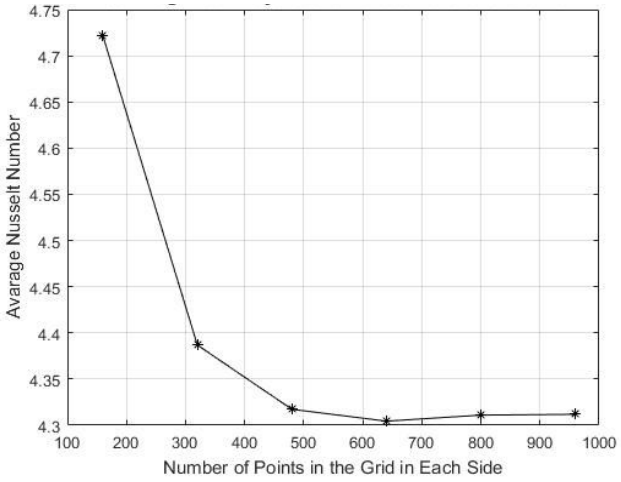

Figure 2. Convergence Analysis as a Function of the Grid Size.

As observed, the number of nodes in the grid in each side of the cavity was changed from 160 to 960. A convergence pattern is seen starting from the mesh with 480 nodes per side. After doing the same analysis for different Reynolds and Prandtl number cases, it was determined that the grid size of 640 is representative for all simulations. As a consequence, the results presented in next sections for this were performed using this mesh size.

A similar procedure was executed for the study with the methodology 2, and 1025 nodes per side of the cavity were assumed to generate numerical results presented in next sections.

3.2 Local and Average Nusselt Numbers

The results for the local Nusselt number in the walls of the square cavity for the two adopted methodologies are shown on Fig 3. Following the procedure done by Mioralli *et al.* (2017), the results are plotted against the S coordinate system along the walls. The intervals S = (0, 0.25) and (2, 2.25) corresponds to the inlet and outlet ports, respectively, where local Nusselt number is not defined. Due to the boundary conditions imposed, the temperature gradient from wall to fluid goes to infinity close to the inlet port, forcing the local Nusselt to diverge. As a consequence, the second methodology achieved higher Nusselt numbers close to the inlet port, since a finer mesh was used in this methodology, meaning that nodes closer to the port were obtained in comparison with the first methodology. It is also observed that the local Nusselt goes to zero near the left bottom and right top corners.

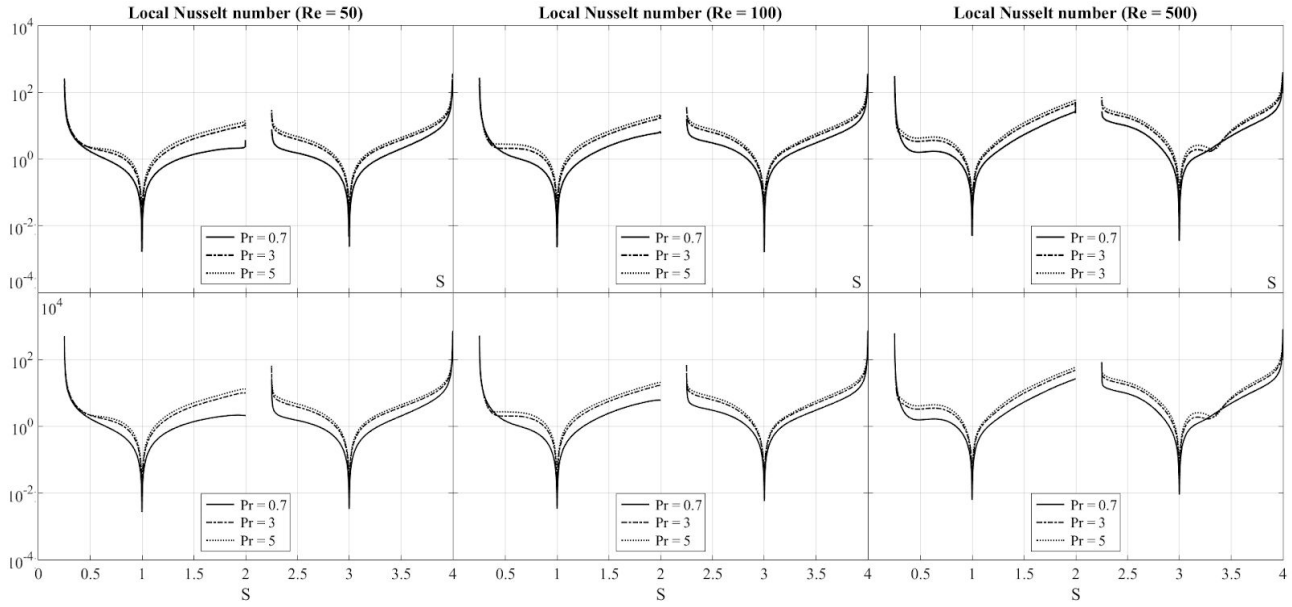

Figure 3. Comparison of local Nusselt between methodology 1 (top line) and methodology 2 (bottom line).

Comparing results from the two methodologies, one can observe that the general behavior of the curves are similar. Also, comparing these approaches with Mioralli *et al.* (2017), it is observed great accordance in the curves trends. Another result studied in this work is the average Nusselt number for mesh sizes of 640 and 1025 nodes per cavity side, for the two thermal approaches and for each Reynolds and Prandtl number, as shown in Tab. 1.

Table 1. Average Nusselt number calculated using methodology 1 and 2, presented in this work .

Re/Pr	Pr = 0.7		Pr = 3.0		Pr = 5.0	
	Methodology 1	Methodology 2	Methodology 1	Methodology 2	Methodology 1	Methodology 2
Re = 50	3.0817	3.2084	5.4226	5.2592	6.3307	6.1074
Re = 100	4.3045	4.2452	7.2958	6.8022	8.5421	7.9474
Re = 500	9.6021	7.9795	14.676	12.785	18.551	15.144

The relative difference between the two methodologies for the local Nusselt number can be seen in Tab. 2. It is observed that results obtained in the two cases have smaller differences at lower Reynolds number flows and increasing discrepancies for higher Reynolds numbers. The energy model presented by Guo *et al.* (2007) was tested for low Reynolds number flows and the validity of the model for higher values of this dimensionless parameter is not established. This fact can be an influence of the differences observed between the two methodologies. The values obtained using the first methodology presented are closer to the ones obtained by Mioralli *et al.* (2017) for the same values of Reynolds and Prandtl numbers. Both methodologies predicted an increase of the average Nusselt as Reynolds and Prandtl numbers increases.

Table 2. Relative difference between average Nusselt numbers from methodology 1 and 2.

Re/Pr	Pr = 0.7	Pr = 3.0	Pr = 5.0
Re = 50	4%	3%	4%
Re = 100	1%	7%	7%
Re = 500	17%	13%	18%

3.3 Streamlines, Temperature Field and Coefficient of Pressure Drop

The velocity and temperature fields were obtained for the Prandtl numbers of 0.7, 3 and 5, and Reynolds numbers of 50, 100 and 500. Figure 4 presents the streamlines and the temperature field obtained from the performed numerical simulations. Two rotating vortices are present at the upper right and bottom left regions of the domain. As expected,

these rotating vortices grows as the Reynolds number increases, which means inertial effects becomes more relevant to the flow. Also, establishment of a secondary vortice is observed in the bottom-left corner for higher Reynolds numbers.

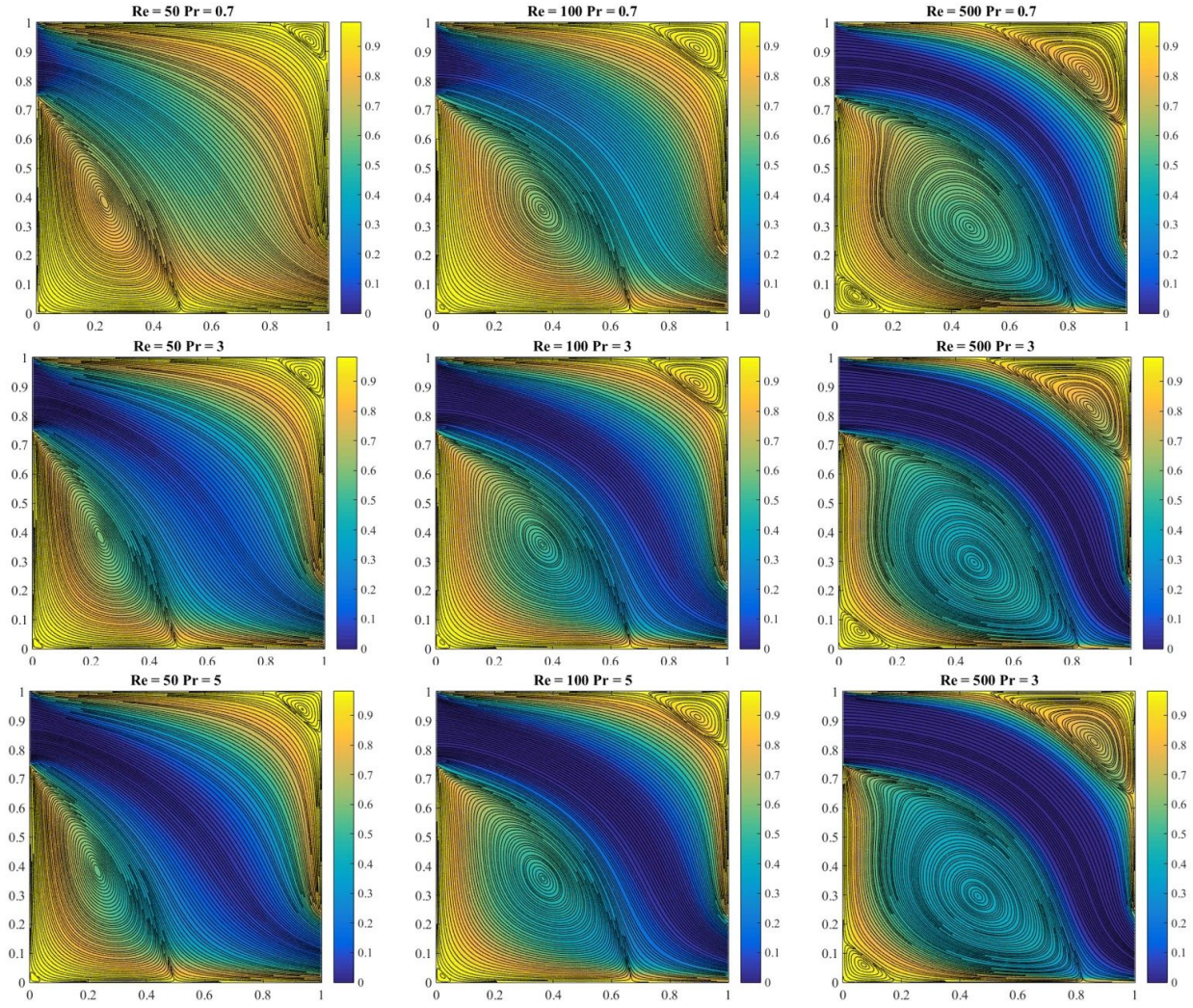

Figure 4. Streamlines and temperature field for Reynolds number equal to 50, 100 and 500 and constant Prandtl number equal to 0.7, 3 and 5.

It is noticed that the vortices increases the fluid mixing inside the cavity. In this way, for stronger vortices, it is observed lower fluid temperatures near the walls, which increases the temperature gradients in these regions. This fact is corroborated by the average Nusselt number analysis. Since the intensity of the vortices depends on the Reynolds number, it is expected that this parameter have a great influence on the average Nusselt number, as observed earlier.

The effect of the increasing of Prandtl number is associated with the increase of Péclet number, which is related the ratio between the advection and diffusion effects. For higher Péclet numbers, advection effects are more relevant in comparison with diffusion effects. In this sense, it is expected that the fluid that follows the streamlines linking the inlet port to the outlet port exhibit a lower temperature rise, as the Prandtl number increases. Both methodologies were able to reproduce this behaviour.

In Tab. 3, results of the dimensionless pressure drop are shown. It can be observed that it is an inverse function of the Reynolds number and independent of the Prandtl number, as the present study is dealing with incompressible flows, in which case the hydrodynamics are decoupled from the thermal effects.

Table 3. Dimensionless pressure drop computed using methodology 1 and 2.

Re/Pr	Pr = 0.7		Pr = 3.0		Pr = 5.0	
	Methodology 1	Methodology 2	Methodology 1	Methodology 2	Methodology 1	Methodology 2
Re = 50	4.6865	5.1549	4.6865	5.1549	4.6865	5.1549
Re = 100	3.0749	3.3874	3.0749	3.3873	3.0749	3.387
Re = 500	1.9604	2.0758	1.9604	2.0759	1.9604	2.0759

4. CONCLUSIONS

In this work, two methodologies of the Thermal Lattice Boltzmann Method (TLBM) were applied to solve the thermo-hydraulic phenomena inside a square cavity under different flow conditions. The methodologies were developed considering the Chapman-Enskog Expansion, in order to ensure that the Navier-Stokes and Energy Equations were correctly solved. These distinct approaches were confronted first considering the local Nusselt number and later for the average Nusselt number. Excellent agreement were observed for low Reynolds number and higher errors were noticed when the Reynolds number was increased. Results of streamlines and temperature field were presented and were in accordance with results available in the literature. Finally, the dimensionless pressure drop was computed and results showed coherence with what is expected from fluid mechanics theory. Based on the presented results, it is shown that Lattice Boltzmann Method can correctly solve the thermal flow inside a square cavity under different conditions. In addition, this methodology can be easily applied to similar problems.

5. ACKNOWLEDGMENTS

This work is supported by Fundação de Amparo à Pesquisa do Estado de São Paulo (FAPESP, grant: 2016/095090-1).

6. REFERENCES

Bejan, A., 1980. “A synthesis of analytical results for natural convection heat transfer across rectangular enclosures”.*International Journal of Heat Mass Transfer*, Vol. 23, pp. 723–726.

Brès, G., Pérot, F. and Freed, D., 2009. “Properties of the lattice boltzmann method for acoustics”. In *15th AIAA/CEAS Aeroacoustics Conference (30th AIAA Aeroacoustics Conference)*. p. 3395.

Chen, H., Orszag, S.A., Staroselsky, I. and Succi, S., 2004. “Expanded analogy between boltzmann kinetic theory of fluids and turbulence”. *Journal of Fluid Mechanics*, Vol. 519, pp. 301–314.

Chen, S., Luo, K. and Zheng, C., 2012. “A simple enthalpy-based lattice boltzmann scheme for complicated thermal systems”. *Journal of Computational Physics*, Vol. 231, No. 24, pp. 8278–8294.

Ginzburg, I., 2005. “Equilibrium-type and link-type lattice Boltzmann models for generic advection and anisotropic-dispersion equation”. *Advances in water resources*, 28(11), 1171-1195.

Ginzburg, I., Verhaeghe, F. and d’Humieres, D. , 2008. “Two-relaxation-time lattice Boltzmann scheme: About parametrization, velocity, pressure and mixed boundary conditions”. *Communications in computational physics*, 3(2), 427-478.

Guangwu, Y., Yaosong, C. and Shouxin, H., 1999. “Simple lattice boltzmann model for simulating flows with shock wave”. *Physical review E*, Vol. 59, No. 1, p. 454.

Guo, Z. and Zhao, T., 2002. “Lattice boltzmann model for incompressible flows through porous media”. *Physical Review E*, Vol. 66, No. 3, p. 036304.

Guo, Z., Zheng, C., Shi, B. and Zhao, T., 2007. “Thermal lattice boltzmann equation for low mach number flows: decoupling model”. *Physical Review E*, Vol. 75, No. 3, p. 036704.

He, X., Chen, S. and Doolen, G.D., 1998. “A novel thermal model for the lattice boltzmann method in incompressible limit”. *Journal of Computational Physics*, Vol. 146, No. 1, pp. 282–300. doi:10.1006/jcph.1998.6057.

He, X., Chen, S. and Zhang, R., 1999. “A lattice boltzmann scheme for incompressible multiphase flow and its application in simulation of rayleigh–taylor instability”. *Journal of Computational Physics*, Vol. 152, No. 2, pp. 642–663.

Krüger, T., Kusumaatmaja, H., Kuzmin, A., Shardt, O., Silva, G. and Viggen, E.M., 2017. *The Lattice Boltzmann Method: Principles and Practice*. Springer International Publishing.

Ladd, A. J. C. and Verberg, R., 2001. "Lattice-Boltzmann simulations of particle-fluid suspensions". *Journal of statistical physics*, v. 104, n. 5-6, p. 1191-1251.

Lallemand, P. and Luo, L.S., 2003. "Theory of the lattice boltzmann method: Acoustic and thermal properties in two and three dimensions". *Physical review E*, Vol. 68, No. 3, p. 036706.

Mioralli, P., Scalon, V., Avallone, E. and Verdério Júnior, S., 2017. "Analysis of laminar forced convection inside a square ventilated cavity using the openfoam". *Engenharia Térmica (Thermal Engineering)*, Vol. 16, No. 1, pp. 66–74.

Peng, Y., Shu, C. and Chew, Y., 2003. "Simplified thermal lattice boltzmann model for incompressible thermal flows". *Physical Review E*, Vol. 68, p. 026701.

Tang, G. H., Tao, W. Q., and He, Y. L., 2005. "Thermal boundary condition for the thermal lattice Boltzmann equation". *Physical Review E*, 72(1), 016703.

Yu, H., Girimaji, S.S. and Luo, L.S., 2005. "DNS and LES of decaying isotropic turbulence with and without frame rotation using lattice boltzmann method". *Journal of Computational Physics*, Vol. 209, No. 2, pp. 599–616.

7. RESPONSIBILITY NOTICE

The author(s) is (are) the only responsible for the printed material included in this paper.